Title

Robust empirical relationships for estimating the carbonate system in the southern California Current System and application to CalCOFI hydrographic cruise data (2005–2011)

Journal

Journal of Geophysical Research, 117(C5)

ISSN

0148-0227

Authors

Alin, Simone R
Feely, Richard A
Dickson, Andrew G
et al.

Publication Date

2012-05-01

DOI

10.1029/2011jc007511

Peer reviewed

Robust empirical relationships for estimating the carbonate system in the southern California Current System and application to CalCOFI hydrographic cruise data (2005–2011)

Simone R. Alin,[1] Richard A. Feely,[1] Andrew G. Dickson,[2] J. Martín Hernández-Ayón,[3] Lauren W. Juranek,[1,4,5] Mark D. Ohman,[2] and Ralf Goericke[2]

Received 17 August 2011; revised 7 February 2012; accepted 6 April 2012; published 22 May 2012.

[1] The California Current System (CCS) is expected to experience the ecological impacts of ocean acidification (OA) earlier than most other ocean regions because coastal upwelling brings old, CO_2-rich water relatively close to the surface ocean. Historical inorganic carbon measurements are scarce, so the progression of OA in the CCS is unknown. We used a multiple linear regression approach to generate empirical models using oxygen (O_2), temperature (T), salinity (S), and sigma theta (σ_θ) as proxy variables to reconstruct pH, carbonate saturation states, carbonate ion concentration ($[CO_3^{2-}]$), dissolved inorganic carbon (DIC) concentration, and total alkalinity (TA) in the southern CCS. The calibration data included high-quality measurements of carbon, oxygen, and other hydrographic variables, collected during a cruise from British Columbia to Baja California in May–June 2007. All resulting empirical relationships were robust, with r^2 values >0.92 and low root mean square errors. Estimated and measured carbon chemistry matched very well for independent data sets from the CalCOFI and IMECOCAL programs. Reconstructed CCS pH and saturation states for 2005–2011 reveal a pronounced seasonal cycle and inter-annual variability in the upper water column. Deeper in the water column, conditions are stable throughout the annual cycle, with perennially low pH and saturation states. Over sub-decadal time scales, these empirical models provide a valuable tool for reconstructing carbonate chemistry related to ocean acidification where direct observations are limited. However, progressive increases in anthropogenic CO_2 content of southern CCS water masses must be carefully addressed to apply the models over longer time scales.

Citation: Alin, S. R., R. A. Feely, A. G. Dickson, J. M. Hernández-Ayón, L. W. Juranek, M. D. Ohman, and R. Goericke (2012), Robust empirical relationships for estimating the carbonate system in the southern California Current System and application to CalCOFI hydrographic cruise data (2005–2011), *J. Geophys. Res.*, *117*, C05033, doi:10.1029/2011JC007511.

1. Introduction

[2] The uptake of anthropogenic CO_2 by the surface oceans has led to declining surface ocean pH and carbonate saturation states globally, through the process of ocean acidification (OA) [*Caldeira and Wickett*, 2003; *Doney et al.*, 2009; *Feely et al.*, 2009, 2004; *Orr et al.*, 2005]. Water masses in the North Pacific Ocean are naturally rich in CO_2, as a result of being at the terminus of the global ocean thermohaline circulation system [*Broecker and Peng*, 1982]. These water masses are thus characterized by water chemistry with relatively lower pH and calcium carbonate saturation states (Ω) than many other areas of the world oceans. As a result, the California Current System (CCS) is poised to experience the impacts of OA on ecological communities sooner than other regions, particularly because the process of upwelling brings deeper water masses (~50–250 m deep) [*Chhak and Di Lorenzo*, 2007], rich in CO_2, to the ocean surface in this region.

[1]NOAA Pacific Marine Environmental Laboratory, Seattle, Washington, USA.
[2]Scripps Institution of Oceanography, University of California, San Diego, La Jolla, California, USA.
[3]Instituto de Investigaciones Oceanológicas, Universidad Autonoma de Baja California, Ensenada, Mexico.
[4]Joint Institute for the Study of the Atmosphere and Ocean, University of Washington, Seattle, Washington, USA.
[5]Now at College of Earth, Ocean, and Atmospheric Sciences, Oregon State University, Corvallis, Oregon, USA.

Corresponding author: S. R. Alin, NOAA Pacific Marine Environmental Laboratory, 7600 Sand Point Way NE, Seattle, WA 98115, USA. (simone.r.alin@noaa.gov)

0148-0227/12/2011JC007511

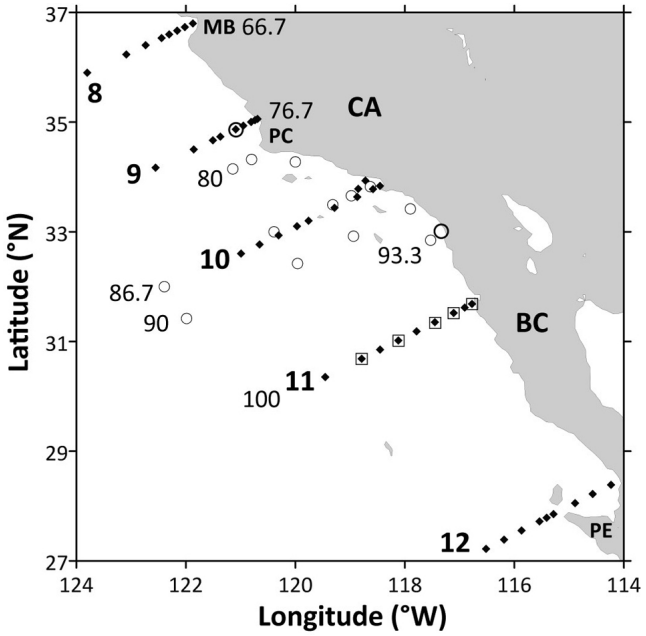

Figure 1. Map of transects and stations from the North American Carbon Program West Coast Cruise (WCC) in 2007 from which the calibration data set was collected (solid diamond symbols). CalCOFI stations where verification samples were collected are indicated with open circles, and IMECOCAL verification sampling locations are shown with open squares. Numbers next to each line of stations represent transect numbers that correspond to WCC stations (bold) and CalCOFI and IMECOCAL transects (regular text). CA, California; BC, Baja California; MB, Monterey Bay; PC, Point Conception; PE, Punta Eugenia. The larger, thick open circles show the location of the time series stations shown in Figures 7 (CalCOFI line 76.7, station 55) and 8 (CalCOFI line 93.3, station 26.7).

[3] Recent time series of data collected in the CCS show trends toward increasing CO_2 concentrations and declining pH since 1993, with an inferred parallel decline in Ω values for the two dominant mineral forms of calcium carbonate, aragonite (Ω_{arag}) and calcite (Ω_{calc}) [*Borges et al.*, 2009; *Wootton et al.*, 2008]. However, within the period of record, inter-annual variability driven by climatic changes in ocean circulation is substantially larger than the trend of increasing CO_2 due to ocean acidification [*Borges et al.*, 2009, Figure 2]. To accurately characterize the past trajectory of ocean acidification in the CCS, it is necessary to rely on models supported by observations of proxy variables that can provide robust estimates of the state of the carbonate system. A method for reconstructing pH and Ω values can yield insight into the seasonality and ultimately the longer-term rate of ocean acidification in coastal CCS waters [cf. *Feely et al.*, 2008b; *Juranek et al.*, 2009].

[4] Longer time series exist for non-carbon oceanographic variables in the CCS, such as temperature (T), salinity (S), and oxygen (O_2) concentrations. The California Cooperative Oceanic Fisheries Investigations (CalCOFI) program has conducted frequent hydrographic (T, S, O_2, and other variables) and biological surveys of the CCS since 1949, with quarterly cruises throughout the southern sector (Monterey Bay south through San Diego waters) since 1984. The CalCOFI time series has generated insights into long-term changes in O_2 concentrations in the southern CCS, including shoaling of the hypoxic boundary between 1984 and 2006 [*Bograd et al.*, 2008], which should correspond to shoaling of low pH, low Ω water masses as well. Though the depth of the hypoxic boundary has oscillated throughout the CalCOFI 60-plus year time series record, it is unclear whether the recent shoaling trend in the hypoxic boundary (and inferred for low pH, low Ω waters) will reverse as seen in earlier decades [*McClatchie et al.*, 2010] or continue to shoal as predicted by coupled physical-biogeochemical circulation models [*Rykaczewski and Dunne*, 2010]. Long-term declines in water column transparency and increases in nitrate concentrations have been documented in this region [*Aksnes and Ohman*, 2009], as well as changes in zooplankton composition [*Lavaniegos and Ohman*, 2007]. The CCS is home to rich marine fish and shellfish populations, which play important ecological and economic roles in the region, and the ecological consequences of shoaling hypoxic and acidified waters could be significant as habitat space on and above the continental shelf becomes increasingly limiting [e.g., *McClatchie et al.*, 2010].

[5] Here we develop empirical equations for estimating the state of the carbonate system—specifically pH, Ω, dissolved inorganic carbon (DIC), total alkalinity (TA), and carbonate ion concentrations ($[CO_3^{2-}]$)—from proxy hydrographic variables for the southern CCS. These predictive relationships can be applied at sub-decadal time scales to estimate carbonate system parameters when direct measurements of carbon chemistry are not available or cost-effective.

2. Study Region

[6] The CCS is comprised of an equatorward-flowing California Current (CC), a seasonally poleward-flowing Inshore Countercurrent (IC) derived from the CC, and a poleward-flowing California Undercurrent (CU) [*Hickey*, 1998; *Lynn and Simpson*, 1987]. The CC originates in the subarctic North Pacific Ocean, is characterized by relatively fresh (S = 33–34), oxygen-rich ($[O_2] > 100$ μmol kg^{-1}) water and constitutes a relatively shallow flow at the surface (0–300 m depth), with the core of its flow 200–300 km offshore [*Lynn and Simpson*, 1987]. The nearshore IC flows poleward predominantly in the fall and winter and is a narrow current typically comprised of water from the CC that has turned shoreward and poleward due to seasonal winds. The CU is a subsurface current (strongest flow at 100–300 m depth) that flows poleward along the continental shelf/slope, originates in the eastern equatorial Pacific Ocean, and is comprised of relatively salty (S > 34), oxygen-poor ($[O_2] <$ 100 μmol kg^{-1}) water [*Gay and Chereskin*, 2009].

[7] The southern CCS, for the purposes of this paper, is considered to consist of the region along the North American west coast from Monterey Bay, California (37°N), south to Punta Eugenia, Baja California (27°N) (Figure 1). This range includes the areas sampled most frequently by CalCOFI from 1949 to the present and the northern half of the transects sampled regularly by Investigaciones Mexicanas

de la Corriente de California (IMECOCAL) from 1997 to the present.

[8] The southern CCS encompasses three sub-regions with differing seasonal circulation dynamics: central California (Monterey Bay to Point Conception), the Southern California Bight (SCB, from Point Conception to roughly the U.S.-Mexico border), and northern Baja California (the U.S.-Mexico border south to Punta Eugenia) [*Lynn and Simpson*, 1987]. However, in all three sub-regions, equatorward winds along the coast can drive upwelling of deeper water masses (frequently the oxygen-poor, nutrient-rich CU) in the nearshore environment, typically in spring throughfall months. Eddy circulation in the SCB can also bring deeper isopycnals closer to the surface during summer and fall months.

3. Data Sets

[9] The calibration data set used for developing the empirical relationships was collected during the North American Carbon Program West Coast Cruise (WCC), which occurred in May–June 2007 [*Feely et al.*, 2008a; *Feely and Sabine*, 2011]. The WCC transects used in the development of the proxy relationships included lines 8–12, extending from Monterey Bay, California, to Punta Eugenia, Baja California (Figure 1). All samples collected between 15 and 500 m water depth at the 46 stations on these transects were included in the calibration data set (n = 692). Independent verification samples were collected during quarterly CalCOFI cruises in 2008–2010 (n = 279) and during 14 IMECOCAL cruises between 2006 and 2008 (n = 72) (Figure 1).

[10] For the calibration and verification data sets, the requirement for inclusion of samples was the availability of high-quality CTD measurements of temperature, salinity, and pressure, and high-quality water column measurements of TA, DIC, and dissolved O_2 concentrations. For all samples, DIC was analyzed coulometrically, following the method of *Johnson et al.* [1985, 1987]. The precision and accuracy of DIC analyses are on the order of ± 2 μmol kg^{-1}. Total alkalinity was quantified using the potentiometric titration method [*Dickson et al.*, 2003]. The precision and accuracy of TA analyses are on the order of ± 3 μmol kg^{-1}. With data for two inorganic carbon parameters (here using DIC and TA), T, and S, we used CO2SYS to calculate all other inorganic carbon parameters at in situ temperatures, including pH (seawater scale), Ω_{arag}, Ω_{calc}, and $[CO_3^{2-}]$ [*Lewis and Wallace*, 1998; *Pierrot et al.*, 2006]. Phosphate and silicate concentrations were available for most samples, and these values were included in the CO2SYS calculations. Oxygen samples were analyzed by the modified Winkler method [*Anderson*, 1971; *Carpenter*, 1965]. Estimated precision for O_2 analyses is $\sim$0.9 μmol kg^{-1} [*Scripps Institution of Oceanography*, 2007].

4. Development and Verification of Empirical Relationships

[11] *Juranek et al.* [2009] developed an empirical relationship for estimating the value of aragonite saturation state in the northern CCS (nCCS) using T and O_2 data as proxy parameters. Key assumptions underpinning this approach are that the stoichiometry of the CO_2:O_2 relationship in the constituent water masses is controlled primarily by aerobic respiration that has occurred in these water masses in the few decades since they were last exposed to the atmosphere and that upwelling is the main process that controls the exposure of the continental shelf to these water masses. The approach and reasoning are described in detail in *Juranek et al.* [2009] and *Kim et al.* [2010]. Here we apply this approach to the southern CCS (sCCS), and extend it to allow the robust estimation of pH, Ω_{calc}, DIC, TA, and $[CO_3^{2-}]$ in addition to Ω_{arag}, using T, O_2, S, and σ_θ data as proxy variables. We also expand the depth coverage of the empirical relationships to 15–500 m water depth (from 30 to 300 m in *Juranek et al.* [2009]), to facilitate the assessment of interactions between inorganic carbon chemistry and biological activity in near-surface waters. The method has not been extended to the ocean surface because differential exchange rates of CO_2 and O_2 at the air-sea interface will alter the CO_2:O_2 ratio in the water and thus violate one of the core assumptions behind the empirical relationships, which depend on a linear relationship between dissolved inorganic carbon and O_2. In addition, surface heat absorption or loss will alter the relationship between temperature and estimated variables, and may bias estimates.

[12] Saturation states for the carbonate biominerals aragonite and calcite are calculated as

$$\Omega_{phase} = \left[Ca^{2+}\right]\left[CO^{2-}\right]/K'_{sp}, \quad (1)$$

where K'_{sp} is the apparent stoichiometric solubility product for the aragonite or calcite mineral phase of calcium carbonate and is governed by in situ temperature, salinity, and pressure conditions. Accurate pH and saturation states can be calculated from high-quality DIC and TA data. In the open ocean, DIC has been approximated as a function of some combination of T, S, nitrate (NO_3^-) or O_2 concentrations, and mixed layer depth [*Anderson and Sarmiento*, 1994; *Barbero et al.*, 2011; *Lee et al.*, 2000], and TA as a function of T and S [*Lee et al.*, 2006].

[13] We tested combinations of the variables T, S, O_2, NO_3^-, and σ_θ using forward and backward stepwise multiple linear regressions to identify the strongest predictive variables for estimating pH, Ω_{arag}, Ω_{calc}, TA, DIC, and $[CO_3^{2-}]$ in the southern CCS. We tested all independent variables for collinearity using pairwise regression and the variance inflation factor (VIF) test with an upper cutoff value of 10 indicating excessive collinearity [*Kutner et al.*, 2004]. The variables with less predictive power that were deemed to be collinear were eliminated. All empirical relationships had very robust statistics for the calibration data set, with low root mean square errors (RMSE) and high r^2 values (>0.92) for all carbonate system parameters (Table 1).

[14] The best predictors for pH, Ω_{arag}, Ω_{calc}, and $[CO_3^{2-}]$ were the independent variables T and O_2, and with an added interaction term, T $\times$ O_2, to reduce bias in the residuals, as in *Juranek et al.* [2009]. To reduce the magnitude of the product of T $\times$ O_2 and resultant errors in the least squares regression analysis, we subtracted a mean reference value

Table 1. Best Empirical Models for pH, Aragonite Saturation, Calcite Saturation, Total Alkalinity, Dissolved Inorganic Carbon, and Carbonate Ion Concentration for the CalCOFI Sampling Region (27°N–37°N) Using Temperature, Oxygen, Salinity, and Sigma Theta as Proxy Variables[a]

Equation	Parameter[b]	VIF[c]	First Parameter Selected in Model	Variance Explained by First Parameter	Final r^2	RMSE	RMCVE	Coefficients ± SE
I	$pH^{est} = \alpha_0 + \alpha_1 (T - T_r) + \alpha_2 (O_2 - O_{2,r}) + \alpha_3 [(T - T_r) \times (O_2 - O_{2,r})]$	4.4, 3.8, 1.3	O_2	96%	0.980	0.024	0.024	$\alpha_0 = 7.758 \pm 0.001$ $\alpha_1 = 1.42 \times 10^{-2} \pm 7.4 \times 10^{-4}$ $\alpha_2 = 1.62 \times 10^{-3} \pm 2.2 \times 10^{-5}$ $\alpha_3 = 4.24 \times 10^{-5} \pm 5.2 \times 10^{-6}$
II	$\Omega_{arag}^{est} = \alpha_0 + \alpha_1 (T - T_r) + \alpha_2 (O_2 - O_{2,r}) + \alpha_3 [(T - T_r) \times (O_2 - O_{2,r})]$	4.4, 3.8, 1.3	T	90%	0.988	0.062	0.063	$\alpha_0 = 1.112 \pm 0.003$ $\alpha_1 = 9.59 \times 10^{-2} \pm 1.6 \times 10^{-3}$ $\alpha_2 = 3.54 \times 10^{-3} \pm 4.9 \times 10^{-5}$ $\alpha_3 = 5.91 \times 10^{-4} \pm 1.1 \times 10^{-5}$
III	$\Omega_{calc}^{est} = \alpha_0 + \alpha_1 (T - T_r) + \alpha_2 (O_2 - O_{2,r}) + \alpha_3 [(T - T_r) \times (O_2 - O_{2,r})]$	4.4, 3.8, 1.3	T	89%	0.988	0.097	0.099	$\alpha_0 = 1.749 \pm 0.005$ $\alpha_1 = 0.147 \pm 0.003$ $\alpha_2 = 5.61 \times 10^{-3} \pm 7.8 \times 10^{-5}$ $\alpha_3 = 8.02 \times 10^{-4} \pm 1.9 \times 10^{-5}$
IV	$TA^{est} = \alpha_0 + \alpha_1 (T - T_r) + \alpha_2 (S - S_r) + \alpha_3 [(T - T_r) \times (S - S_r)]$	2.0, 2.0, 1.1	S	84%	0.927	6.4	6.4	$\alpha_0 = 2246.67 \pm 0.31$ $\alpha_1 = -3.70 \pm 0.14$ $\alpha_2 = 67.79 \pm 1.02$ $\alpha_3 = -13.28 \pm 0.41$
V	$DIC^{est} = \alpha_0 + \alpha_1 (\sigma_\theta - \sigma_{\theta,r}) + \alpha_2 (O_2 - O_{2,r}) + \alpha_3 [(\sigma_\theta - \sigma_{\theta,r}) \times (O_2 - O_{2,r})]$	8.1, 7.1, 1.4	σ_θ	95%	0.988	9.5	9.6	$\alpha_0 = 2165.76 \pm 0.54$ $\alpha_1 = 80.75 \pm 1.57$ $\alpha_2 = -0.45 \pm 0.012$ $\alpha_3 = -0.052 \pm 0.0087$
VI	$[CO_3^{2-}]^{est} = \alpha_0 + \alpha_1 (T - T_r) + \alpha_2 (O_2 - O_{2,r}) + \alpha_3 [(T - T_r) \times (O_2 - O_{2,r})]$	4.4, 3.8, 1.3	T	89%	0.987	4.2	4.3	$\alpha_0 = 73.94 \pm 0.21$ $\alpha_1 = 5.85 \pm 0.12$ $\alpha_2 = 0.23 \pm 0.0035$ $\alpha_3 = 0.040 \pm 0.00084$

[a] Ω_{arag}, aragonite saturation; Ω_{calc}, calcite saturation; TA, total alkalinity; DIC, dissolved inorganic carbon; $[CO_3^{2-}]$, carbonate ion concentration; T, temperature; O_2, oxygen; S, salinity; σ_θ, sigma theta.

[b] $O_{2,r}$, T_r, S_r, and $\sigma_{\theta,r}$ for the calibration data set were 138.46 μmol kg^{-1}, 10.28°C, 33.889, and 26.01 kg m^{-3}, respectively.

[c] VIF, variance inflation factor (see text).

from each independent variable. The final form of the empirical equations for these dependent variables was

$$pH^{est}\left(\text{or } \Omega^{est} \text{ or } \left[CO_3^{2-}\right]^{est}\right) = \alpha_0 + \alpha_1(T - T_r) + \alpha_2\left(O_2 - O_{2,r}\right) + \alpha_3(T - T_r) \times \left(O_2 - O_{2,r}\right), \quad (2)$$

where pH^{est}, Ω^{est}, and $[CO_3^{2-}]^{est}$ are the estimated proxy values of pH, Ω, and $[CO_3^{2-}]$; all α terms are model-estimated coefficients; and the subscript r denotes a reference value, in this case the mean for the calibration data set (Table 1). The best empirical relationship for TA included the variables S and T, as well as an interaction term (S × T), and took the form

$$TA^{est} = \alpha_0 + \alpha_1(T - T_r) + \alpha_2(S - S_r) + \alpha_3(T - T_r) \times (S - S_r). \quad (3)$$

[15] Finally, the strongest relationship for DIC was with σ_θ, O_2, and an interaction term ($\sigma_\theta \times O_2$) and was in the form

$$DIC^{est} = \alpha_0 + \alpha_1\left(\sigma_\theta - \sigma_{\theta,r}\right) + \alpha_2\left(O_2 - O_{2,r}\right) + \alpha_3\left(\sigma_\theta - \sigma_{\theta,r}\right) \times \left(O_2 - O_{2,r}\right). \quad (4)$$

[16] Consistency of the calibration data set was assessed through cross-validation analysis, in which the calibration data set was randomly divided into 10 equal subsets, a regression model was created with 9/10 of the data, and the performance of the model was tested by comparing the predicted and observed values for the other 1/10 of the data set. Root mean cross-validation error (RMCVE) values were essentially identical to the RMSE values for the whole data set, indicating consistency across the calibration data set (Table 1).

[17] Estimates of pH and Ω could also be calculated from DIC and TA estimates, although it is simpler to use the direct equations to estimate these parameters. The RMSEs for TA and DIC are two to four times higher than measurement error for laboratory analyses of TA and DIC, so we would expect somewhat greater error to be introduced to estimates of pH and Ω by using estimated DIC and TA to calculate them. *Juranek et al.* [2011] found that the uncertainty was similar for pH and Ω whether they were calculated directly or from DIC and TA estimates, but the error around their DIC estimate was much smaller than in this study (±3.5 versus ±9.5 μmol kg^{-1}).

[18] As an independent means of verification, the empirical relationships were applied to O_2, T, S, and σ_θ data from

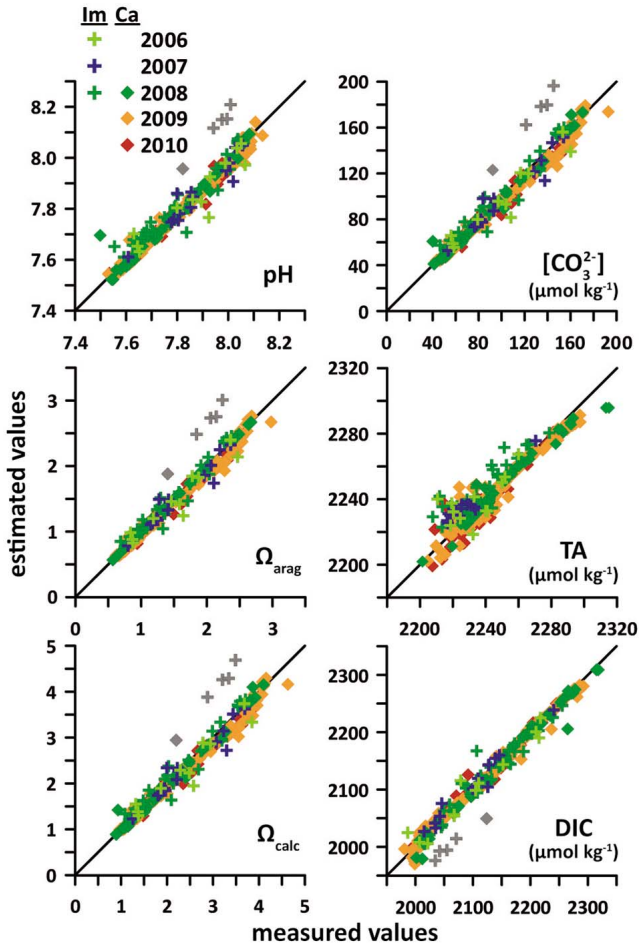

Figure 2. Measured versus estimated values of pH, aragonite saturation (Ω_{arag}), calcite saturation (Ω_{calc}), carbonate ion concentration ($[CO_3^{2-}]$), total alkalinity (TA), and dissolved inorganic carbon concentration (DIC) for all verification samples. Black lines represent a 1:1 relationship. CalCOFI (Ca) data are shown in diamonds and IMECOCAL (Im) data are represented by pluses, with different colors for each sampling year as shown in the key. Outliers are shown in gray.

the CalCOFI and IMECOCAL verification data sets collected between 2006 and 2010. Plots of observed versus predicted values for all verification samples indicate excellent agreement of model estimates of pH, Ω_{arag}, Ω_{calc}, TA, DIC, and $[CO_3^{2-}]$ with measured values (Figure 2). Agreement is weakest for TA, with a looser correlation at the low end of the range (measured TA < 2260 μmol kg^{-1}) as well as a tendency for the relationship to underestimate TA at the high end of the range (TA > 2280 μmol kg^{-1}). The loose relationship between measured and estimated values is at the shallow end of the depth range (15–30 m) and is likely explained by a combination of biological calcification processes and/or input of freshwater. Regressions between measured and estimated values for all carbonate system parameters for pooled CalCOFI and IMECOCAL verification data had r^2 values of 0.96–0.98 and regression slopes (m) of 0.97–0.98, with the exception of TA (r^2 = 0.93, m = 0.87). Four samples were outliers (visually detected) on all plots except TA, and were not included in the regressions (gray symbols in Figure 2).

[19] We compared the skill of our Ω_{arag} relationship (i.e., equation II in Table 1) for the sCCS with that of *Juranek et al.* [2009] for the nCCS by applying both relationships to the full suite of CalCOFI and IMECOCAL verification samples (n = 352). We found that there was a mean offset of 0.19 between the observed Ω_{arag} values and those calculated using the nCCS relationship, with the *Juranek et al.* [2009] relationship consistently underestimating Ω_{arag} in the sCCS, particularly at low Ω_{arag} values. To determine the cause of this offset, we generated an empirical relationship for the entire CCS with the same final structure as equation II and tested it on the combined CalCOFI/IMECOCAL sample set. We found that the full CCS relationship had very similar coefficients and performed essentially identically to equation II for this sCCS sample set, although the overall model RMSE was higher (0.091). (Note: We have not addressed how well the full CCS model would perform relative to an independent nCCS sample set, as it is outside the scope of this study.) The two main differences between the nCCS relationship and equation II are a smaller intercept for the nCCS relationship (0.9242 versus 1.112) and the lack of a temperature term in the nCCS model. We suspect that the lack of a temperature term drives the observed offset, as the mean temperatures over the calibration data set for the nCCS (WCC lines 3–5) and sCCS (WCC lines 8–12) relationships are substantially different (8.61°C versus 10.28°C, respectively). Mean values for other proxy variables also differ sufficiently between the calibration data sets for the nCCS ($[O_2]_{mean}$ = 181.2 μmol kg^{-1}, $\sigma_{\theta,mean}$ = 25.76 kg m^{-3}, and S_{mean} = 33.26) and the sCCS ($[O_2]_{mean}$ = 138.5 μmol kg^{-1}, $\sigma_{\theta,mean}$ = 26.01 kg m^{-3}, and S_{mean} = 33.89) that careful analysis of the coefficients for all relationships must be undertaken to extend the applicability of equations I–VI generated here (Table 1) for the sCCS to the nCCS. The difference in means between regions reflects the greater contribution and shallower depth of California Undercurrent water in the sCCS than in the nCCS [*Chhak and Di Lorenzo*, 2007; *Thomson and Krassovski*, 2010].

[20] In developing the empirical relationships in Table 1, tradeoffs were evaluated between minimizing RMSE values and maximizing the geographic coverage of the relationships. We expected that the empirical relationship for estimating aragonite saturation would be similar between the northern and southern CCS, but because no calibration data from locations south of Trinidad Head in northern California were used in generating the *Juranek et al.* [2009] Ω_{arag} relationship, it was necessary to reevaluate the coefficients of the relationship. Further, many important drivers of carbon cycle processes differ in magnitude between the northern and southern CCS: continental shelf width [*Chase et al.*, 2007], primary production [*Hickey and Banas*, 2008], terrestrial inputs [*Chase et al.*, 2007], and average upwelling intensity (http://www.pfeg.noaa.gov/products/pfel/modeled/indices/upwelling/NA/click_map.html). In addition, despite the presence of the same constituent water masses in the northern and southern CCS, evolution of temperature and O_2 characteristics of the major currents occurs during transit along the coast. All of these factors may influence the values

of the coefficients or the relative importance of a proxy parameter. As an example, *Juranek et al.* [2011] found that the North Pacific Ocean required distinct relationships for estimating carbonate system parameters in the subarctic and subtropical gyres because the drivers of carbon cycling in the two sub-basins differ substantially.

5. Application of Empirical Relationships: Temporal and Spatial Variability in the Carbonate System in the Southern CCS (2005–2011)

[21] The empirical relationships were subsequently applied to O_2, T, S, and σ_θ data collected between 15 and 500 m water depth on all CalCOFI cruises between January 2005 and January 2011 to generate proxy hindcast values for pH^{est}, Ω^{est}_{arag}, Ω^{est}_{calc}, TA^{est}, DIC^{est}, and $[CO_3^{2-}]^{est}$. Here we focus our discussion on observed magnitudes and variability of pH and saturation states, and we use DIC and TA records to interpret the influence of biological activity on pH and Ω values. Reconstructed Ω_{arag} and pH values at 20 and 30 m show seasonal variability, with higher maxima during summer and to a lesser extent fall when biological drawdown of CO_2 in warm surface waters leads to higher pH and Ω values (Table 2 and Figure 3). The range of pH^{est} and Ω^{est} values at 20 and 30 m tends to be largest in summer and smallest in winter, indicating that spatial variability across the CalCOFI region is typically strongest in summer and weakest in winter. The widest range of estimated DIC and TA values occur during spring and summer across the time series, coinciding with the seasonal peaks of upwelling and biological production, respectively, both of which can drive strong gradients of organic and inorganic carbon concentrations in the euphotic zone (Table 2). Mean DIC^{est} concentrations during summer and fall are lowest, reflecting biological drawdown, which is apparently sufficient to overcome the signal of increased DIC due to upwelling of deeper CO_2-rich water masses on average (Table 2). Mean TA is higher during summer and fall, suggesting that upwelling of water masses with higher TA overwhelms any signal of biological carbonate production that might reduce TA in the surface ocean (Table 2). On average, oxygen concentrations at this depth tend to be highest in winter, likely as a result of surface ocean mixing, re-aeration, and temperature-driven solubility effects, while average summer conditions are marked by great variability, as a result of the complex interplay between primary production producing O_2 and upwelling or eddy formation bringing O_2-poor waters to the surface (Table 2).

[22] At depths of 75 and 125 m, spatial variability is still substantial, as indicated by the wide range of pH^{est} and Ω^{est} values observed on all cruises, but variability is not as strongly tied to the seasonal cycle (Figure 3). At 75 m, the highest and lowest cruise-wide averages for pH^{est} and Ω^{est} frequently co-occur with highs or lows for T or O_2, but at 125 m, O_2 shows stronger covariability with pH^{est} and Ω^{est} than T, as T variability is diminished at this depth (Table S1).[1] At 300 m and deeper, both variability and values of pH^{est} and Ω^{est} are low throughout the time series, indicating perennially corrosive conditions with limited spatial, seasonal, and inter-annual variability (Figure 3 and Tables 2 and S1). At this depth, corresponding values of DIC^{est} and TA^{est} are high and variability low (Tables 2 and S1).

[23] The order of parameter selection in the regressions also indicates which independent variable (T, S, O_2, σ_θ) offers the most explanatory power for the variance in the dependent variable (pH^{est}, Ω^{est}_{arag}, Ω^{est}_{calc}, TA^{est}, DIC^{est}, $[CO_3^{2-}]^{est}$). For pH^{est}, the first parameter selected by the model was O_2, whereas for Ω^{est} and $[CO_3^{2-}]^{est}$, T was selected first (Table 1). For TA and DIC, S and σ_θ were the parameters explaining the most variability in the models, respectively (Table 1). Covariation between the predictor variables (T, O_2) and the estimated variables (pH^{est}, Ω^{est}) in cruise-wide averages (Table S1) and in the full data set (not shown) further confirm that Ω^{est}_{arag} and Ω^{est}_{calc} are more strongly influenced by T, whereas pH^{est} is more strongly influenced by O_2. Thus, Ω appears to be more strongly tied to temperature-driven changes in calcium carbonate solubility, while pH is more responsive to biological and physical processes affecting the stoichiometry of O_2 and CO_2 concentrations. Comparing relationships among predictor and estimated variables across depths reveals that the strength of the relationship between O_2 and estimated variables increases with depth, whereas the strength of T versus pH^{est} or Ω^{est} relationships diminishes with depth as T variability diminishes (Tables 2 and S1). Near-surface processes (heating and gas exchange) can explain some of this pattern. At the surface, temperature ranges are largest due to seasonal heating of surface water masses. Gas exchange will tend to alter the stoichiometric relationship between O_2 and CO_2 because O_2 reaches equilibrium with the atmosphere more rapidly than CO_2, so water masses closer to the surface that may be affected by gas exchange would not have as strong a relationship between O_2 and pH^{est} or Ω^{est}. In addition, shifting contributions of CC and CU water masses with depth likely contribute to the observed tradeoff between the importance of T and O_2 influence.

[24] To illustrate patterns of spatial variability in the state of the carbonate system through the southern CCS, we plotted pH^{est}, Ω^{est}_{arag} and Ω^{est}_{calc} proxy values on 20, 75, 125, and 300 m depth surfaces for CalCOFI cruises characterized by large and small ranges in observed proxy values (Figures 4 and 5, time windows selected are indicated by vertical gray and black lines, respectively, in Figure 3). For both Ω^{est}_{arag} and pH^{est}, the widest range of values was observed during the summer of 2005, and the smallest range was observed during the winter of 2010. During the high-variability summer 2005 CalCOFI cruise, spatial patterns in reconstructed pH, Ω_{arag}, and Ω_{calc} showed the strongest gradients along an onshore-offshore axis, with the lowest estimated values of pH and saturation states present nearshore at each depth (Figure 4). In the upper few hundred meters, pH^{est} varied from 7.71 to 8.08 at 20 m ($\Delta_{max-min} = 0.37$), from 7.65 to 8.07 at 75 m ($\Delta = 0.42$), and from 7.62 to 7.98 ($\Delta = 0.36$), with the strongest onshore-offshore gradient at intermediate depth. At 300 m depth, pH variability spanned a range of 7.55–7.69 ($\Delta = 0.13$). Aragonite saturation estimates varied from 1.01 to 2.88 on the 20 m depth surface ($\Delta = 1.87$), from 0.84 to 2.67 at 75 m ($\Delta = 1.83$), and from 0.78 to 2.00 at 125 m depth ($\Delta = 1.22$), with values and variability

[1] Auxiliary materials are available in the HTML. doi:10.1029/2011JC007511.

Table 2. Average Seasonal Values (and Ranges) for Measured and Estimated Variables Across All January 2005–January 2011 CalCOFI Cruises at Selected Depths

	Measured				Estimated					
Season	Temperature (°C)	Salinity	Sigma Theta (kg m^{-3})	Oxygen (μmol kg^{-1})	pH^{est}	Aragonite Saturation, Ω^{est}_{arag}	Calcite Saturation, Ω^{est}_{calc}	Total Alkalinity (μmol kg^{-1})	Dissolved Inorganic Carbon (μmol kg^{-1})	Carbonate Ion Concentration (μmol kg^{-1})
					Depth 20 m					
Winter	13.92 (11.2–17.4)	33.27 (32.7–33.7)	24.86 (24.2–25.7)	256.63 (179.8–316.8)	8.02 (7.84–8.13)	2.13 (1.39–2.59)	3.33 (2.18–4.02)	2229.0 (2198.3–2246.6)	2026.9 (1979.6–2120.9)	139.3 (91.5–167.9)
Spring	13.58 (9.3–16.7)	33.32 (32.8–34.1)	24.97 (24.3–26.3)	253.52 (89.6–308.5)	8.01 (7.67–8.11)	2.08 (0.89–2.51)	3.24 (1.40–3.91)	2230.3 (2201.4–2261.0)	2036.1 (1987.8–2209.8)	135.7 (59.8–163.3)
Summer	15.33 (10.2–19.8)	33.37 (32.7–33.9)	24.60 (23.7–26.1)	246.87 (109.7–339.5)	8.03 (7.71–8.20)	2.32 (1.01–3.00)	3.62 (1.58–4.65)	2240.9 (2204.8–2268.3)	2012.4 (1941.3–2180.7)	151.2 (67.2–194.0)
Autumn	16.21 (11.3–19.5)	33.35 (32.8–33.8)	24.42 (23.7–25.6)	246.28 (152.4–290.3)	8.04 (7.80–8.11)	2.44 (1.29–2.84)	3.80 (2.03–4.41)	2243.2 (2217.3–2261.4)	1998.2 (1950.2–2124.4)	158.7 (85.1–183.6)
					Depth 30 m					
Winter	13.76 (10.7–17.4)	33.27 (32.7–33.7)	24.90 (24.2–25.8)	250.81 (155.0–283.2)	8.01 (7.79–8.05)	2.08 (1.21–2.58)	3.25 (1.90–4.02)	2228.5 (2194.9–2246.5)	2031.8 (1981.2–2144.4)	135.9 (80.3–167.8)
Spring	13.29 (9.2–16.7)	33.33 (32.8–34.1)	25.03 (24.3–26.4)	243.00 (73.5–282.0)	7.98 (7.64–8.05)	1.98 (0.82–2.51)	3.10 (1.28–3.91)	2229.5 (2198.3–2266.0)	2045.7 (1988.8–2227.0)	129.6 (55.3–163.2)
Summer	14.41 (9.7–19.6)	33.37 (32.7–33.9)	24.80 (23.7–26.2)	236.61 (84.9–298.8)	7.99 (7.67–8.12)	2.12 (0.90–2.87)	3.32 (1.42–4.46)	2237.2 (2190.8–2262.9)	2031.6 (1948.7–2200.0)	138.7 (60.5–185.8)
Autumn	15.55 (10.6–19.5)	33.34 32.8–33.8)	24.56 (23.7–25.8)	240.30 (121.9–275.4)	8.02 (7.73–8.09)	2.31 (1.08–2.84)	3.59 (1.69–4.41)	2240.1 (2214.5–2261.4)	2010.6 (1951.4–2157.5)	150.1 (71.6–183.8)
					Depth 75 m					
Winter	11.96 (9.1–17.3)	33.38 (32.7–34.0)	25.32 (24.3–26.2)	203.07 (91.4–263.2)	7.89 (7.68–8.05)	1.60 (0.93–2.58)	2.51 (1.46–4.01)	2223.4 (2179.6–2253.7)	2084.6 (1991.4–2199.0)	105.2 (62.0–167.3)
Spring	11.84 (8.5–16.7)	33.44 (32.8–34.1)	25.39 (24.4–26.5)	202.57 (59.6–284.7)	7.89 (7.61–8.05)	1.60 (0.75–2.51)	2.51 (1.19–3.91)	2227.5 (2186.1–2270.9)	2089.5 (1993.2–2240.6)	105.4 (51.6–163.4)
Summer	11.62 (8.8–17.6)	33.47 (32.7–34.1)	25.44 (24.3–26.4)	194.56 (72.4–271.5)	7.88 (7.64–8.07)	1.54 (0.83–2.67)	2.42 (1.31–4.16)	2229.0 (2153.9–2265.8)	2097.3 (1983.5–2222.3)	101.5 (56.2–173.5)
Autumn	11.84 (9.4–17.4)	33.39 (32.8–33.9)	25.36 (24.2–26.2)	201.23 (77.5–270.2)	7.89 (7.67–8.08)	1.58 (0.91–2.68)	2.47 (1.43–4.18)	2223.0 (2182.3–2249.5)	2088.0 (1976.4–2198.2)	103.6 (61.2–174.4)
					Depth 125 m					
Winter	10.06 (8.4–14.1)	33.68 (33.0–34.1)	25.91 (25.0–26.4)	151.63 (77.0–249.2)	7.78 (7.65–8.01)	1.15 (0.83–2.12)	1.81 (1.31–3.31)	2233.8 (2190.4–2264.9)	2152.3 (2040.5–2222.4)	76.7 (56.3–138.4)
Spring	10.05 (8.3–15.4)	33.69 (32.9–34.2)	25.92 (25.0–26.5)	152.21 (49.6–262.7)	7.78 (7.60–8.01)	1.16 (0.72–2.25)	1.83 (1.14–3.50)	2235.4 (2183.9–2274.6)	2152.7 (2040.1–2250.5)	77.4 (49.6–146.2)
Summer	10.03 (8.4–15.4)	33.73 (32.9–34.2)	25.95 (25.0–26.5)	149.15 (57.0–251.9)	7.77 (7.61–8.04)	1.15 (0.76–2.35)	1.82 (1.19–3.66)	2238.8 (2177.1–2276.2)	2157.4 (2042.0–2241.1)	76.8 (51.6–153.0)
Autumn	9.70 (88–13.9)	33.81 (33.1–34.1)	26.08 (24.9–26.4)	130.23 (74.8–240.1)	7.74 (7.64–7.99)	1.04 (0.83–2.01)	1.64 (1.30–3.15)	2243.8 (2199.1–2263.5)	2175.4 (2037.7–2223.2)	69.8 (56.0–131.7)
					Depth 300 m					
Winter	7.67 (6.4–9.0)	34.14 (34.0–34.3)	26.65 (26.5–26.8)	62.47 (22.2–153.1)	7.61 (7.55–7.74)	0.71 (0.63–0.90)	1.12 (1.00–1.43)	2276.4 (2260.4–2289.0)	2254.2 (2199.5–2278.3)	49.0 (44.4–31.2)

Table 2. (continued)

	Measured				Estimated					
Season	Temperature (°C)	Salinity	Sigma Theta (kg m^{-3})	Oxygen (μmol kg^{-1})	pH^{est}	Aragonite Saturation, Ω^{est}_{arag}	Calcite Saturation, Ω^{est}_{calc}	Total Alkalinity (μmol kg^{-1})	Dissolved Inorganic Carbon (μmol kg^{-1})	Carbonate Ion Concentration (μmol kg^{-1})
Spring	7.64	34.14	26.66	64.59	7.61	0.71	1.12	2276.8	2253.7	49.2
	(6.4–9.1)	(34.0–34.3)	(26.5–26.8)	(25.6–136.2)	(7.55–7.72)	(0.63–0.90)	(0.99–1.42)	(2260.8–2294.4)	(2214.8–2283.6)	(44.2–61.0)
Summer	7.67	34.15	26.66	60.07	7.60	0.70	1.11	2277.1	2255.7	48.7
	(6.5–9.6)	(34.0–34.4)	(26.4–26.8)	(24.4–129.2)	(7.55–7.71)	(0.63–0.86)	(0.99–1.36)	(2259.9–2291.3)	(2211.7–2281.6)	(44.4–58.5)
Autumn	7.53	34.11	26.65	65.30	7.61	0.71	1.11	2274.1	2252.7	48.9
	(6.7–8.4)	(34.0–34.3)	(26.5–26.8)	(17.4–107.9)	(7.54–7.67)	(0.62–0.81)	(0.98–1.28)	(2261.5–2287.9)	(2224.1–2277.9)	(43.6–55.4)

continuing to decrease with depth to a range of 0.64–0.82 at 300 m (Δ = 0.19) (Figure 4). Calcite saturation across each depth surface ranged from 1.58 to 4.47 at 20 m (Δ = 2.89), from 1.33 to 4.16 at 75 m (2.83), from 1.23 to 3.13 at 125 m (Δ = 1.90), and finally from 1.00 to 1.30 at 300 m (Δ = 0.30). During the summer, upwelling of CO_2-rich subsurface water masses brings low-pH and low-Ω water masses into nearshore surface waters north and south of Point Conception. Upwelling and eddy formation in the Southern California Bight both act to steepen the gradients of pH^{est} and Ω^{est} along depth surfaces in shallower water by bringing deeper water masses closer to the surface during spring throughfall months.

[25] In contrast, during the winter 2010 CalCOFI cruise, spatial variability was quite low in reconstructed pH, Ω_{arag} and Ω_{calc} (Figure 5). Variability predominantly reflected differences in oceanographic conditions north and south of Point Conception, with lower estimated values for pH and saturation states north of CalCOFI line 80 (extending off of Point Conception) in the core of the California Current upwelling system and higher values in the Southern California Bight. On average, winter months (DJF) between Monterey Bay and the Southern California Bight are relatively quiescent with respect to upwelling, with only episodic bursts of upwelling or downwelling activity (36° and 33°N plots on http://www.pfeg.noaa.gov/products/PFEL/modeled/indices/upwelling/NA/daily_upwell_graphs.html). Estimated winter 2010 pH values were much less variable across the depth surfaces in Figure 5, with a range of 7.99–8.05 at 20 m depth (Δ = 0.06), 7.82–8.04 at 75 m depth (Δ = 0.22), and 7.73–7.97 at 125 m depth (Δ = 0.25). In contrast to the summer variability maps, depth-surface variability during this winter cruise increased with depth between 20 and 125 m, with very low variability at 20 m reflecting wintertime wind mixing and weaker stratification. pH variability at 300 m depth was the same as during summer 2005 (7.55–7.69, Δ = 0.13) with essentially the same mean, which only varies from 7.60 to 7.61 throughout the time series (Figure 3 and Table S1), indicating that seasonal and inter-annual variability are not strong at this depth. Aragonite saturation ranges from 1.97 to 2.52 along the 20 m depth surface (Δ = 0.55), from 1.24 to 2.37 at 75 m (Δ = 1.13), and from 0.96 to 1.87 at 125 m depth (Δ = 0.90), with peak variability at 75 m, and values and variability falling at 300 m (0.65–0.80, Δ = 0.15). Calcite saturation followed the same pattern as aragonite with ranges of 3.09–3.93 at 20 m (Δ = 0.84), 1.96–3.69 at 75 m (Δ = 1.73), 1.52–2.92 at 125 m (Δ = 1.40), and 1.02–1.27 at 300 m (Δ = 0.25). Together, the maps for high- and low-gradient CalCOFI cruises delineate the envelope of variability seen in pH and saturation states in the southern CCS between 2005 and 2011. While the variability in all parameters is relatively low in the low-variability snapshot (i.e., Figure 5), it is well within the ability of the empirical relationships to resolve the variability at all depths (Table 1).

[26] Seasonal shifts in isopycnal depths and the associated pH^{est} and Ω^{est} conditions may have ramifications for living organisms. Depth profiles (15–500 m) from quarterly cruises along CalCOFI line 86.7 in 2005 reveal the magnitude of depth migration of pH^{est} and Ω^{est}_{arag} surfaces during an annual cycle (Figure 6). Under winter conditions (January 2005), pH^{est} and Ω^{est}_{arag} isopleths are horizontal along most of the onshore-offshore transect, with deepening of the surfaces

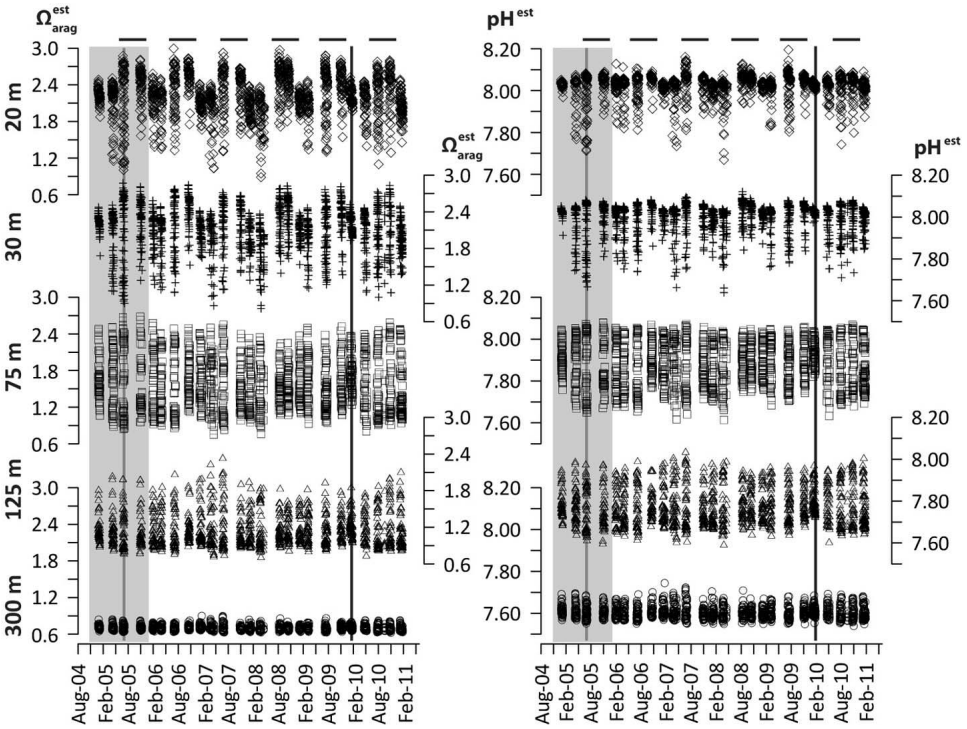

Figure 3. Time series for proxy (left) aragonite saturation (Ω^{est}_{arag}) and (right) pH^{est} values for CalCOFI cruises between January 2005 and January 2011 at standard CalCOFI sampling depths of 20, 30, 75, 125, and 300 m. Within each cruise, the spread of the data reflects the spatial variability of Ω^{est}_{arag} and pH^{est} at each depth. Black dashes at the top of the figure indicate timing of summer and fall cruises for all years. The vertical gray line marks the summer 2005 CalCOFI cruise (high spatial variability, Figure 4), and the vertical black line denotes the winter 2010 cruise (low spatial variability, Figure 5). The shaded gray region highlights all 2005 CalCOFI cruises, which are profiled in Figure 6 to show the seasonal variability of pH^{est} and Ω^{est}_{arag} with depth.

from station 90 offshore (~450 km offshore). During the spring 2005 CalCOFI cruise, pH^{est} and Ω^{est}_{arag} isopleths begin to slope upward. Summer to fall conditions in 2005 were influenced by the strong expression of the Southern California Eddy, centered on stations 45 and 50, which caused the upward doming of pH^{est} and Ω^{est}_{arag} surfaces nearshore relative to their spring depth distribution [*Peterson et al.*, 2006]. Between January and July 2005, upward doming caused the aragonite saturation horizon (ASH, $\Omega^{est}_{arag} = 1$) to shoal by ~100 m from 150 to 200 m to ~25–70 m in the nearshore region (between stations 33 and 50). This indicates that calcifying aragonitic organisms living in the upper 100 m of the water column experienced corrosive conditions for some or all of the spring to fall upwelling season in some locations.

[27] On the sub-decadal time scale of this time series reconstruction for pH^{est} and Ω^{est}_{arag}, we see clear evidence for seasonal and spatial variability in carbonate chemistry related to OA in the upper few hundred meters of the water column (Figure 3). The depths of pH and Ω_{arag} surfaces appear to oscillate by approximately 100 m through an annual cycle, bringing low pH, low Ω_{arag} water masses near the surface in summertime (Figure 6). The seasonal incursion of the aragonite saturation horizon into the upper 100 m of the water column may have implications for biological productivity in the southern CCS during the summer growing season. In addition, a growing body of evidence suggests that many, but not all, calcareous organisms will experience an increasingly difficult time synthesizing calcium carbonate skeletons, shells, or tests under decreasing saturation states [*Hendriks et al.*, 2010; *Hofmann et al.*, 2010; *Kroeker et al.*, 2010]. The only biological time series of calcareous organisms in the southern CCS showed no decline in abundance of calcareous holozooplankton over the last six decades, although the study was not able to address changes in spatial or depth distributions or shell morphology that may have occurred during the study period [*Ohman et al.*, 2009]. Research on the shoaling hypoxic boundary suggests that the coupled effects of low O_2 and high CO_2 may act to limit habitable benthic substrates for many calcifying and non-calcifying organisms over the coming decades [cf. *McClatchie et al.*, 2010].

[28] Although decadal trends and variability in pH and Ω cannot be evaluated during a time series of this duration, we can gain some insight into inter-annual variability from this reconstruction. In a time series plot for station 55 on line 76.7 (see Figure 1 for location), differences in the annual depth oscillation of pH^{est} and Ω^{est} surfaces are evident across years (Figure 7). The largest seasonal oscillations in depth surfaces at this location occurred during 2005 and 2006, and the

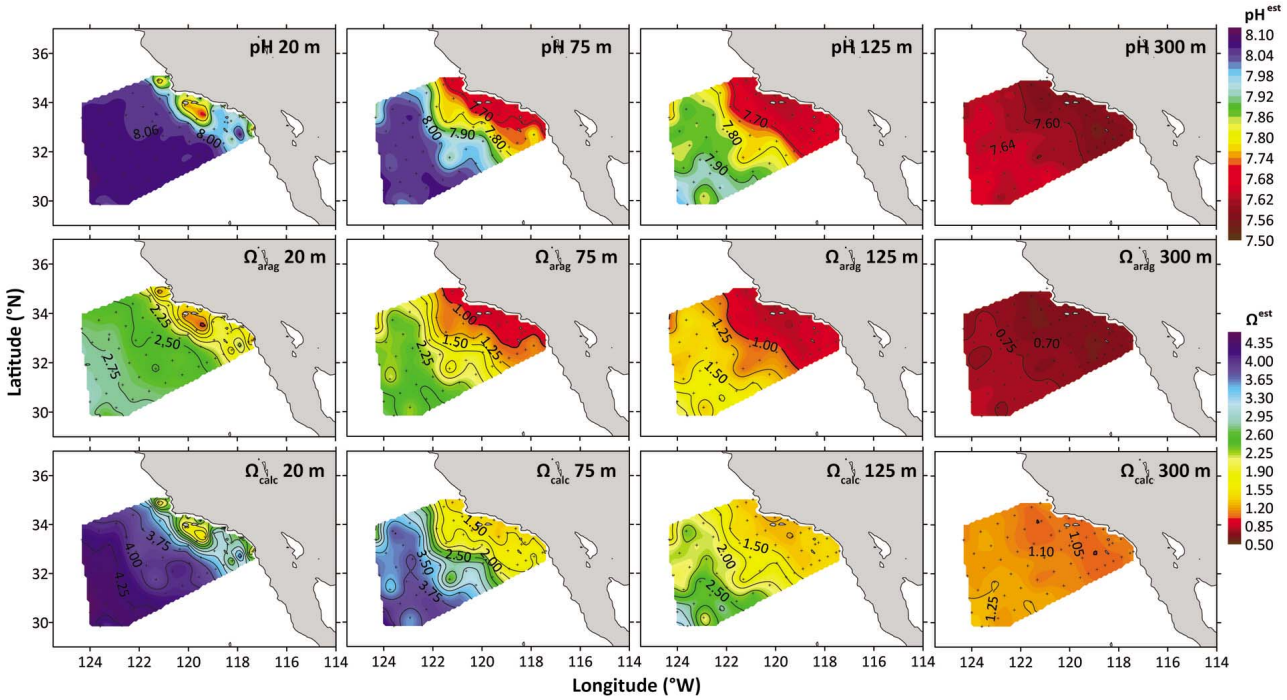

Figure 4. Maps of proxy (top) pH, (middle) aragonite saturation (Ω_{arag}), and (bottom) calcite saturation (Ω_{calc}) at 20, 75, 125, and 300 m for the CalCOFI cruise conducted in summer 2005, a period of high spatial variability. Ω_{arag} and Ω_{calc} share the same color scale. Conditions that are below saturation for Ω_{arag} or Ω_{calc} ($\Omega < 1$) and the corresponding pH values are shown in red, with all other colors representing Ω values above 1.0. The location of Point Conception is shown in Figure 1.

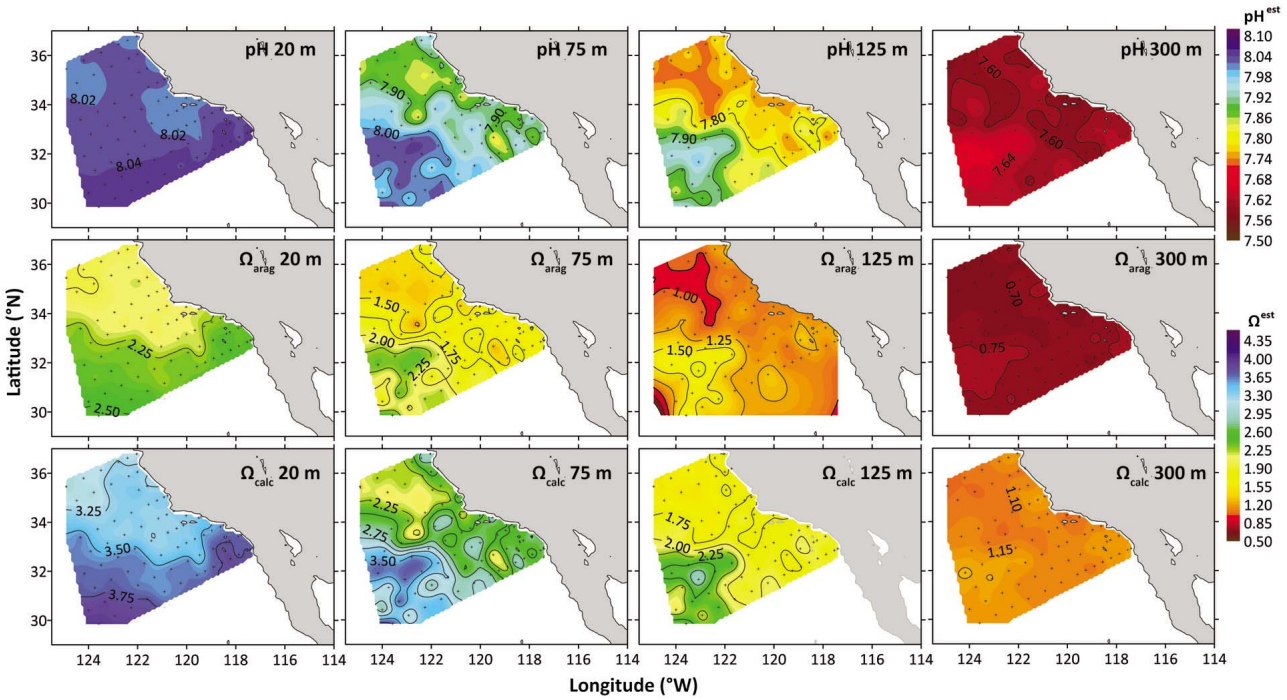

Figure 5. Maps of proxy pH, aragonite saturation, and calcite saturation at 20, 75, 125, and 300 m for the CalCOFI cruise conducted in winter 2010, a period with low spatial variability. Arrangement of figures, color scales, and other details is the same as in Figure 4.

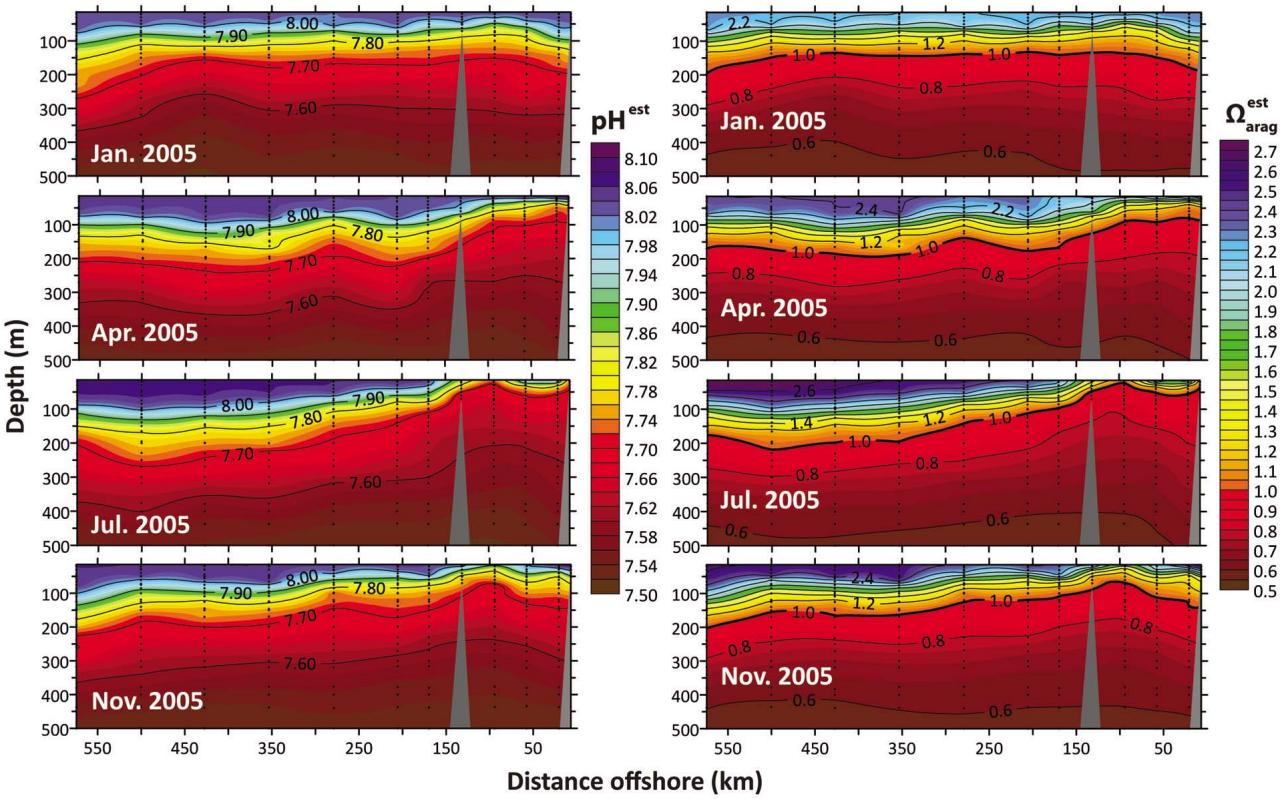

Figure 6. Cross-sections of proxy (left) pH and (right) aragonite saturation for CalCOFI line 86.7 for all seasonal cruises in 2005. Depths shown are from 15 to 500 m. The bathymetric peak between 100 and 150 km offshore represents a shallow sampling station near San Nicolas Island. The true contours near the island are likely more complicated than shown, but those shown in the figure are meant to represent conditions just north of the island.

weakest in 2008. The total magnitude of the seasonal oscillation of the aragonite saturation horizon (ASH) ranged from ~130 m in 2005, when the ASH impinged on the upper 30 m of the water column during the summer, to ~30 m in 2008, when the ASH remained relatively stable around 100 m depth throughout the year. Through the whole time series, the mean depth of the ASH at this location was 136 m (Figure 7). The calcite saturation horizon (Ω^{est}_{calc} = 1) oscillated around an average depth of 382 m at this station, with a smaller amplitude depth oscillation (~20–60 m) through the seasonal cycle. Values of pH^{est} between 15 and 100 m depth ranged from 7.68 to 8.02 during this time series, with values as low as 7.54 at 500 m depth (Figure 7). Corresponding to these conditions, the carbonate ion showed a pronounced concentration gradient from 15 to 500 m (Figure 7). At 20 m, $[CO_3^{2-}]^{est}$ ranged from a low of <70 μmol kg^{-1} (summer 2005) to a high of ~150 μmol kg^{-1} (fall 2006). At depths of 300–500 m, $[CO_3^{2-}]^{est}$ is continually <50 μmol kg^{-1}. TA and DIC values observed during the time series in the 15–100 m depth range were 2210–2260 μmol kg^{-1} and 2040–2200 μmol kg^{-1}, respectively, with the seasonal variation likely reflecting a combination of biogenic carbonate production (ΔTA), biological CO_2 drawdown (ΔDIC), and physical movement of water masses through the water column by upwelling, downwelling, or eddy circulation (Figure 7). Below the euphotic zone, changing isopycnal depths should drive most observed variability in carbonate parameters. This five-year time series demonstrates that the southern CCS experiences pronounced seasonal and inter-annual variability in the depth of pH^{est} and Ω^{est}_{arag} surfaces and other carbonate chemistry parameters. CCS time series stations in Monterey Bay and northern Baja California show suppressed upwelling during warm El Niño anomalies and enhanced upwelling during cold La Niña anomalies [cf. *Borges et al.*, 2009; *Friederich et al.*, 2002; *Linacre et al.*, 2010]. At this CalCOFI time series station, comparison to the Oceanic Niño Index (ONI, http://www.cpc.ncep.noaa.gov/products/analysis_monitoring/ensostuff/ensoyears.shtml) reveals that isopleths are substantially deeper than the 2005–2011 average during El Niño conditions in the first half of 2005 when the ONI was in decline from the July–December 2004 El Niño, the second half of 2006, and the first half of 2010 (Figure 7). The depression of isopleths observed between June 2009 and April 2010, corresponding to the highest values of the ONI (El Niño phase) during this time series, however, was weaker than the response to the weaker El Niño anomalies in July–December 2004 and August 2006–January 2007. The oceanic response to the El Niño of 2009–2010 may be somewhat unusual as it appears to have propagated into the southern California Current region primarily via atmospheric teleconnections rather than through oceanic advection [*Todd et al.*, 2011]. The strongest upwelling of isopleths during the 2005–2011

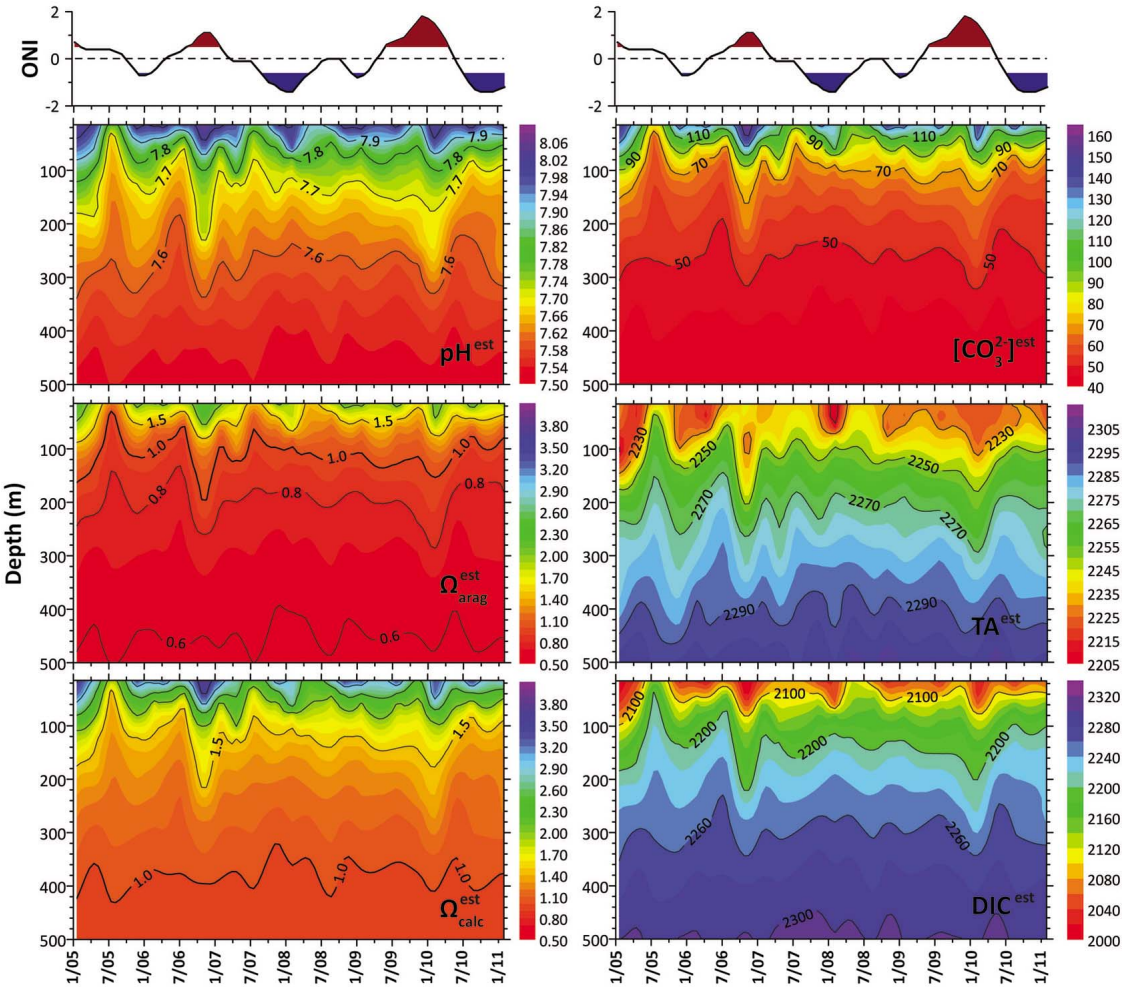

Figure 7. Time series (January 2005–January 2011) of pH^{est}, aragonite saturation (Ω^{est}_{arag}), calcite saturation (Ω^{est}_{calc}), $[CO_3^{2-}]^{est}$, total alkalinity (TA^{est}), and dissolved inorganic carbon (DIC^{est}) for water depths of 15–500 m at station 55 on CalCOFI line 76.7. The Oceanic Niño Index (ONI) time series is shown at the top, with periods meeting the criteria for El Niño anomalies shaded in red, and those for La Niña in blue.

time series at this station was during the spring and summer of 2005, when the ONI index was declining from the 2004 El Niño anomaly. There is no evidence at this station of enhanced upwelling during the La Niña conditions in the second half of 2010.

[29] A five-year mooring time series (2006–2011) study off of northern San Diego, California, examined the 2009–2010 El Niño and 2010–2011 La Niña events in more detail and found evidence for enhanced O_2 depletion and acidity in nearshore, near-surface water masses because of the additional uplifting of isopycnals associated with La Niña conditions [*Nam et al.*, 2011]. We compared a reconstructed time series of carbonate chemistry from the nearest CalCOFI station to the mooring site (line 93.3, station 26.7) (Figure 8). At this station, pronounced deepening of isopleths occurred with respect to all carbonate parameters during the 2009–2010 El Niño, as well as some shoaling of isopleths during the 2010–2011 La Niña relative to preceding years (Figure 8). However, the strongest depression and shoaling of isopleths in this station's time series also occurred in 2005 (prior to the *Nam et al.* [2011] time series) and reflects a response to the weaker El Niño conditions in the second half of 2004. *Nam et al.* [2011] argue that the relatively late seasonal timing of the 2010–2011 La Niña (fall 2010–winter 2011) mitigated its impact on the low-O_2, low-pH event observed, and that the coincidence of La Niña conditions with the normal seasonal peak of upwelling in this region (spring–summer) could result in previously unseen depletions in O_2 and peaks in acidity. The more pronounced fluctuations in isopleth depth observed in response to the weaker 2004 El Niño are consistent with *Nam et al.*'s [2011] interpretation. During the 2005–2011 time series, organisms living at or below ~70 m in the water column at this station experienced undersaturated conditions ($\Omega^{est}_{arag} \leq 1$) for a minimum of about three months each year (e.g., 2008 and 2009). In 2007 and 2010, aragonite undersaturation persisted for roughly six months each year, and corrosive conditions were continuous in the bottom waters at this station from roughly March 2005 to October 2006. The shallowest depth that undersaturated waters reached at this station was ~30–35 m in March–July 2005 (noting the possibility that worse conditions existed during the time series that were

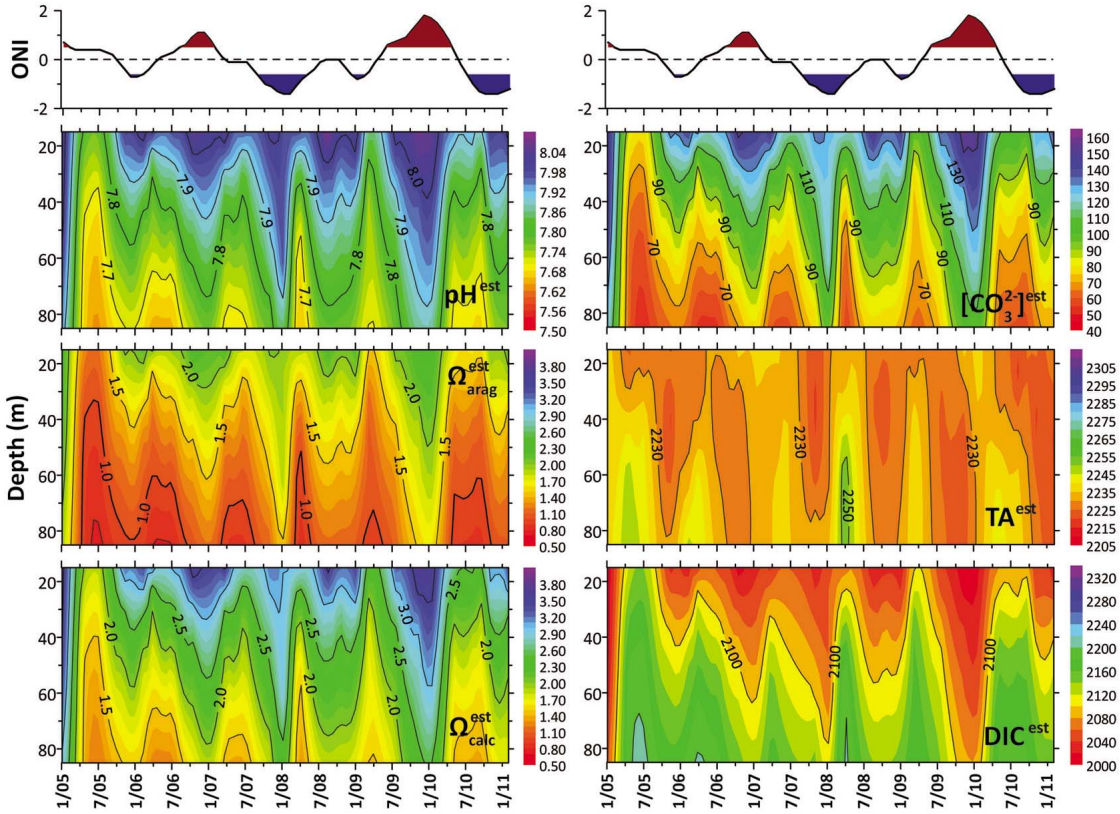

Figure 8. Carbonate system time series (January 2005–January 2011) reconstruction for CalCOFI line 93.3 station 26.7.

not sampled on a CalCOFI cruise and therefore are not accurately represented in Figure 8).

6. Limitations to Applying the Empirical Model

[30] While these empirical models can provide very robust estimates of carbonate system parameters from proxy variables, several aspects of this approach require further research to extend the applicability of this model to the full range of potential data sets. For instance, the length of the reconstructed CalCOFI time series presented here is insufficient to evaluate decadal variability. In order to extend the reconstruction further back in time (e.g., applying the model to the full CalCOFI time series to 1949), it would first be necessary to account for the progressive addition of anthropogenic CO_2 to the water column during the last several decades, as this addition will change the CO_2:O_2 relationship through time [e.g., *Kim et al.*, 2010]. However, physical circulation within the southern CCS is complex [*Hickey*, 1992], and past studies of chlorofluorocarbon (CFC) distributions indicate that corrections for anthropogenic CO_2 penetration within the southern CCS may be difficult [*Min et al.*, 2002]. In order to extend the reconstructions further back in time, a better understanding of the age distribution of water masses within the study area (i.e., the time of last contact with the atmosphere) would be necessary, so that the anthropogenic CO_2 content could be accurately quantified and corrected for in hindcasts extending further back in time. No robust estimates exist for this presently, but the current thinking is that it is on the order of a few decades [*Feely et al.*, 2008a; *Hales et al.*, 2005]. Without further development, analysis by *Juranek et al.* [2011] indicates that the it would take approximately 10 years for the error caused by anthropogenic CO_2 addition to exceed the uncertainty limits of these estimates; thus, the models presented here should be robust for and applicable to the southern CCS during roughly the period 1997–2017 (i.e., date of calibration data set $\pm$10 years). We expect that extending the model significantly beyond this time window will result in proxy estimates with increasing error because of secular changes in concentration of anthropogenic CO_2 in source water masses. Continued collection of calibration and tracer data will allow careful assessment of the actual rate of anthropogenic CO_2 increase in southern CCS water masses and can serve as the basis for long-term reconstructions taking anthropogenic CO_2 contributions into account.

[31] A separate but related issue is that on a decadal scale, large-scale shifts in coastal ocean circulation may affect the depth distribution of the water masses in the CCS, resulting in different chemical signatures in the water masses over the depth zone that these empirical models cover. Detailed information on the long-term variability of the physical and chemical properties of the CCS is required to understand how such inter-annual to decadal changes will affect the state of the carbonate system in our coastal ecosystems. In a recent analysis of the CalCOFI data set, large-scale cooling

and freshening of the water from 50 to 200 m within the California Current was attributed to an enhancement of the amount of cool, lower-salinity subarctic water transported southward from the subarctic North Pacific [*Di Lorenzo et al.*, 2005]. In other examples, West Coast time series of CO_2 and pH data suggest that another significant shift in source water depth distribution may have occurred since 2005 [*Borges et al.*, 2009; *Wootton et al.*, 2008]. Off of northwest Washington, a drop of ~0.4 in summertime average surface pH was observed between 2002 and 2008, which may reflect stronger upwelling of a more acidic water mass than was previously observed [*Wootton et al.*, 2008]. On the Central California coast, the rate of increase in pCO_2 and the rate of pH decrease were substantially higher in surface waters between 2006 and 2008 than the long-term trend (1993–2008) [*Borges et al.*, 2009]. In both cases, the pH declines observed are larger over a shorter period of time than can be explained by the atmospheric accumulation and surface ocean uptake of CO_2 alone. These observations indicate that it is critical to consider circulation processes when assessing ocean acidification in coastal oceans. Earth system models predict large changes in the carbon, oxygen, and macronutrient content of upwelling water masses in the CCS by 2100 [*Rykaczewski and Dunne*, 2010]. Both the steady accumulation of anthropogenic CO_2 in CCS water masses and the potential for large-scale shifts in circulation to affect CCS chemical signatures indicate that it is critical to continue collecting new observations to extend and verify the applicability of these empirical models to new data sets over longer time periods.

[32] Another consideration is that, under hypoxic conditions, the empirical relationships may change as a result of changing respiratory CO_2:O_2 stoichiometry [e.g., *Chen*, 2002]. A recent reassessment of anaerobic remineralization and resulting changes in alkalinity (and thus CO_2:O_2 stoichiometry) in continental shelf settings indicates that upwelling systems such as the CCS may be among the only places where this effect can be significant, albeit just on a local scale [*Hu and Cai*, 2011]. Hypoxic conditions have been observed throughout the CCS increasingly since 2000 [*Bograd et al.*, 2008; *Chan et al.*, 2008; *Grantham et al.*, 2004] and are predicted to increase further by 2100 [*Rykaczewski and Dunne*, 2010], although CalCOFI time series data indicate multidecadal oscillations in the depth of the hypoxic boundary [*McClatchie et al.*, 2010]. In order to keep pace with the changing chemistry of CCS water masses, continued development and verification of these empirical relationships will be necessary over the coming decades.

[33] Finally, river-dominated continental margins such as the U.S. East Coast may present a greater challenge to developing the types of empirical relationship described here. River inputs may be very localized, and individual rivers may have quite different chemical signatures [e.g., *Cai and Wang*, 1998; *Raymond et al.*, 2004], creating a situation with three or more end-members for a model. Except in the case of very large rivers, it may be the case that the influence of the freshwater inputs is limited to parts of the continental shelf or water column that are excluded from this type of approach anyway, due to considerations of surface heating and gas exchange [*Jiang et al.*, 2010]. Enhanced subsurface acidification due to eutrophication driven by river-borne nutrients may still complicate matters by altering CO_2:O_2 relationships [*Cai et al.*, 2011].

7. Conclusions

[34] Empirical models for estimating the parameters pH, Ω_{arag}, and Ω_{calc} using oxygen, temperature, and other hydrographic proxy data provide robust reconstructions of the state of the carbonate system within the southern CCS on sub-decadal time scales and can lend insight into the process of ocean acidification in this upwelling coastal ecosystem. Applying these models to CalCOFI hydrographic data for 2005–2011 revealed seasonal variability in pH and calcium carbonate saturation states and shallower saturation horizons in the summer and fall than during winter and early spring. In addition, spatial variability during summer conditions appears to be dominated by onshore-offshore gradients due to upwelling and eddy formation in the southern CCS, in contrast to winter, when north-south gradients are more prevalent.

[35] These empirical models are robust for reconstructing pH, Ω, and other inorganic carbon parameters at sub-decadal time scales, but for longer reconstructions, it will be necessary to correct for anthropogenic CO_2 increases in the surface ocean. Continued observations are critical for providing a solid observational basis for estimating the effects of this long-term CO_2 accumulation on the empirical relationships, as well as for addressing the potential effects of hypoxia on the underlying CO_2:O_2 relationship.

[36] **Acknowledgments.** We thank the scientists and crew of the 2007 West Coast Cruise for generating a high-quality calibration data set and the scientists and crew of the CalCOFI and IMECOCAL programs (IMECOCAL funded by CONACyT 25339, 23804, 2008–99252) for making their hydrographic time series available. This work was supported by the NOAA Global Carbon Cycle and Ocean Acidification Programs and a contribution from the California Current Ecosystem LTER site, supported by NSF. This publication was partially funded by the Joint Institute for the Study of the Atmosphere and Ocean (JISAO) under NOAA Cooperative Agreement NA10OAR4320148. This is PMEL contribution 3743 and JISAO contribution 2022.

References

Aksnes, D. L., and M. D. Ohman (2009), Multi-decadal shoaling of the euphotic zone in the southern sector of the California Current System, *Limnol. Oceanogr.*, *54*(4), 1272–1281, doi:10.4319/lo.2009.54.4.1272.

Anderson, G. C. (1971), Marine technicians handbook: Oxygen analysis, *Sea Grant Publ. 9*, 29 pp., Scripps Inst. of Oceanogr., La Jolla, Calif.

Anderson, L. A., and J. L. Sarmiento (1994), Redfield ratios of remineralization determined by nutrient data analysis, *Global Biogeochem. Cycles*, *8*(1), 65–80, doi:10.1029/93GB03318.

Barbero, L., J. Boutin, L. Merlivat, N. Martin, T. Takahashi, S. C. Sutherland, and R. Wanninkhof (2011), Importance of water mass formation regions for the air-sea CO_2 flux estimate in the Southern Ocean, *Global Biogeochem. Cycles*, *25*, GB1005, doi:10.1029/2010GB003818.

Bograd, S. J., C. G. Castro, E. Di Lorenzo, D. M. Palacios, H. Bailey, W. Gilly, and F. P. Chavez (2008), Oxygen declines and the shoaling of the hypoxic boundary in the California Current, *Geophys. Res. Lett.*, *35*, L12607, doi:10.1029/2008GL034185.

Borges, A. V., et al. (2009), A global sea surface carbon observing system: Inorganic and organic carbon dynamics in coastal oceans, paper presented at OceanObs'09 Conference, Eur. Space Agency, Venice, Italy, 21–25 Sep.

Broecker, W. S., and T.-H. Peng (1982), *Tracers in the Sea*, Lamont-Doherty Geol. Obs., Palisades, N. Y.

Cai, W.-J., and Y. Wang (1998), The chemistry, fluxes, and sources of carbon dioxide in the estuarine waters of the Satilla and Altamaha Rivers, Georgia, *Limnol. Oceanogr.*, *43*(4), 657–668, doi:10.4319/lo.1998.43.4.0657.

Cai, W.-J., et al. (2011), Acidification of subsurface coastal waters enhanced by eutrophication, *Nat. Geosci.*, *4*, 766–770, doi:10.1038/ngeo1297.

Caldeira, K., and M. E. Wickett (2003), Oceanography: Anthropogenic carbon and ocean pH, *Nature*, *425*(6956), 365, doi:10.1038/425365a.

Carpenter, J. H. (1965), The Chesapeake Bay Institute technique for the Winkler dissolved oxygen method, *Limnol. Oceanogr.*, *10*, 141–143, doi:10.4319/lo.1965.10.1.0141.

Chan, F., J. A. Barth, J. Lubchenco, A. Kirincich, H. Weeks, W. T. Peterson, and B. A. Menge (2008), Emergence of anoxia in the California Current Large Marine Ecosystem, *Science*, *319*(5865), 920, doi:10.1126/science.1149016.

Chase, Z., P. G. Strutton, and B. Hales (2007), Iron links river runoff and shelf width to phytoplankton biomass along the U.S. West Coast, *Geophys. Res. Lett.*, *34*, L04607, doi:10.1029/2006GL028069.

Chen, C. T. A. (2002), Shelf- vs. dissolution-generated alkalinity above the chemical lysocline, *Deep Sea Res., Part II*, *49*, 5365–5375, doi:10.1016/S0967-0645(02)00196-0.

Chhak, K., and E. Di Lorenzo (2007), Decadal variations in the California Current upwelling cells, *Geophys. Res. Lett.*, *34*, L14604, doi:10.1029/2007GL030203.

Dickson, A. G., J. D. Afghan, and G. C. Anderson (2003), Reference materials for oceanic CO_2 analysis: A method for the certification of total alkalinity, *Mar. Chem.*, *80*, 185–197, doi:10.1016/S0304-4203(02)00133-0.

Di Lorenzo, E., A. J. Miller, N. Schneider, and J. C. McWilliams (2005), The warming of the California Current System: Dynamics and ecosystem implications, *J. Phys. Oceanogr.*, *35*(3), 336–362, doi:10.1175/JPO-2690.1.

Doney, S. C., V. J. Fabry, R. A. Feely, and J. A. Kleypas (2009), Ocean acidification: The other CO_2 problem, *Annu. Rev. Mar. Sci.*, *1*, 169–192, doi:10.1146/annurev.marine.010908.163834.

Feely, R., and C. Sabine (2011), Carbon Dioxide and Hydrographic Measurements During the 2007 NACP West Coast Cruise, http://cdiac.ornl.gov/ftp/oceans/NACP_West_Coast_Cruise_2007/, Carbon Dioxide Inf. Anal. Cent., Oak Ridge Natl. Lab., Oak Ridge, Tenn.

Feely, R. A., C. L. Sabine, K. Lee, W. Berelson, J. Kleypas, V. J. Fabry, and F. J. Millero (2004), Impact of anthropogenic CO_2 on the $CaCO_3$ system in the oceans, *Science*, *305*(5682), 362–366, doi:10.1126/science.1097329.

Feely, R. A., C. L. Sabine, J. M. Hernandez-Ayon, D. Ianson, and B. Hales (2008a), Evidence for upwelling of corrosive "acidified" water onto the continental shelf, *Science*, *320*(5882), 1490–1492, doi:10.1126/science.1155676.

Feely, R. A., B. Hales, C. Sabine, D. Greeley, K. Lee, S. Alin, and L. Juranek (2008b), A new proxy method for estimating the aragonite saturation state of coastal waters using chemical and hydrographic data, *Eos Trans. AGU*, *89*(53), Fall Meet. Suppl., Abstract OS33E-03.

Feely, R. A., S. C. Doney, and S. R. Cooley (2009), Ocean acidification: Present conditions and future changes in a high-CO_2 world, *Oceanography*, *22*(4), 36–47, doi:10.5670/oceanog.2009.95.

Friederich, G. E., P. M. Walz, M. G. Burczynski, and F. P. Chavez (2002), Inorganic carbon in the central California upwelling system during the 1997–1999 El Niño-La Niña event, *Prog. Oceanogr.*, *54*, 185–203, doi:10.1016/S0079-6611(02)00049-6.

Gay, P. S., and T. K. Chereskin (2009), Mean structure and seasonal variability of the poleward undercurrent off southern California, *J. Geophys. Res.*, *114*, C02007, doi:10.1029/2008JC004886.

Grantham, B. A., F. Chan, K. J. Nielsen, D. S. Fox, J. A. Barth, A. Huyer, J. Lubchenco, and B. A. Menge (2004), Upwelling-driven nearshore hypoxia signals ecosystem and oceanographic changes in the northeast Pacific, *Nature*, *429*(6993), 749–754, doi:10.1038/nature02605.

Hales, B., T. Takahashi, and L. Bandstra (2005), Atmospheric CO_2 uptake by a coastal upwelling system, *Global Biogeochem. Cycles*, *19*, GB1009, doi:10.1029/2004GB002295.

Hendriks, I. E., C. M. Duarte, and M. Alvarez (2010), Vulnerability of marine biodiversity to ocean acidification: A meta-analysis, *Estuarine Coastal Shelf Sci.*, *86*(2), 157–164, doi:10.1016/j.ecss.2009.11.022.

Hickey, B. M. (1992), Circulation over the Santa Monica-San Pedro basin and shelf, *Prog. Oceanogr.*, *30*, 37–115, doi:10.1016/0079-6611(92)90009-O.

Hickey, B. M. (1998), Coastal oceanography of western North America from the tip of Baja California to Vancouver Island, in *The Sea*, edited by A. R. Robinson and K. H. Brink, pp. 345–393, John Wiley, New York.

Hickey, B. M., and N. S. Banas (2008), Why is the northern end of the California Current System so productive?, *Oceanography*, *21*(4), 90–107, doi:10.5670/oceanog.2008.07.

Hofmann, G. E., J. P. Barry, P. J. Edmunds, R. D. Gates, D. A. Hutchins, T. Klinger, and M. A. Sewell (2010), The effect of ocean acidification on calcifying organisms in marine ecosystems: An organism-to-ecosystem perspective, *Annu. Rev. Ecol. Evol. Syst.*, *41*, 127–147, doi:10.1146/annurev.ecolsys.110308.120227.

Hu, X., and W.-J. Cai (2011), An assessment of ocean margin anaerobic processes on oceanic alkalinity budget, *Global Biogeochem. Cycles*, *25*, GB3003, doi:10.1029/2010GB003859.

Jiang, L.-Q., et al. (2010), Carbonate mineral saturation states along the U.S. East Coast, *Limnol. Oceanogr.*, *55*, 2424–2432, doi:10.4319/lo.2010.55.6.2424.

Johnson, K. M., A. E. King, and J. M. Sieburth (1985), Coulometric TCO_2 analyses for marine studies; an introduction, *Mar. Chem.*, *16*, 61–82, doi:10.1016/0304-4203(85)90028-3.

Johnson, K. M., P. J. Williams, L. Brändström, and J. M. Sieburth (1987), Coulometric TCO_2 analysis for marine studies: Automation and calibration, *Mar. Chem.*, *21*, 117–133, doi:10.1016/0304-4203(87)90033-8.

Juranek, L. W., R. A. Feely, W. T. Peterson, S. R. Alin, B. Hales, K. Lee, C. L. Sabine, and J. Peterson (2009), A novel method for determination of aragonite saturation state on the continental shelf of central Oregon using multi-parameter relationships with hydrographic data, *Geophys. Res. Lett.*, *36*, L24601, doi:10.1029/2009GL040778.

Juranek, L. W., R. A. Feely, D. Gilbert, H. Freeland, and L. Miller (2011), Real-time estimation of pH and aragonite saturation state from Argo profiling floats: Prospects for an autonomous carbon observing strategy, *Geophys. Res. Lett.*, *38*, L17603, doi:10.1029/2011GL048580.

Kim, T.-W., K. Lee, R. A. Feely, C. L. Sabine, C. T. A. Chen, H. J. Jeong, and K. Y. Kim (2010), Prediction of Sea of Japan (East Sea) acidification over the past 40 years using a multiparameter regression model, *Global Biogeochem. Cycles*, *24*, GB3005, doi:10.1029/2009GB003637.

Kroeker, K. J., R. L. Kordas, R. N. Crim, and G. G. Singh (2010), Meta-analysis reveals negative yet variable effects of ocean acidification on marine organisms, *Ecol. Lett.*, *13*(11), 1419–1434, doi:10.1111/j.1461-0248.2010.01518.x.

Kutner, M., C. Nachtsheim, J. Neter, and W. Li (2004), *Applied Linear Regression Models*, McGraw-Hill, Boston.

Lavaniegos, B. E., and M. D. Ohman (2007), Coherence of long-term variations of zooplankton in two sectors of the California Current System, *Prog. Oceanogr.*, *75*(1), 42–69, doi:10.1016/j.pocean.2007.07.002.

Lee, K., R. Wanninkhof, R. A. Feely, F. J. Millero, and T. H. Peng (2000), Global relationships of total inorganic carbon with temperature and nitrate in surface seawater, *Global Biogeochem. Cycles*, *14*(3), 979–994, doi:10.1029/1998GB001087.

Lee, K., L. T. Tong, F. J. Millero, C. L. Sabine, A. G. Dickson, C. Goyet, G. H. Park, R. Wanninkhof, R. A. Feely, and R. M. Key (2006), Global relationships of total alkalinity with salinity and temperature in surface waters of the world's oceans, *Geophys. Res. Lett.*, *33*, L19605, doi:10.1029/2006GL027207.

Lewis, E., and D. W. R. Wallace (1998), Program developed for CO_2 system calculations, *Rep. ORNL/CDIAC-105*, Carbon Dioxide Inf. Anal. Cent., Oak Ridge Natl. Lab., U.S. Dep. of Energy, Oak Ridge, Tenn., doi:10.2172/639712.

Linacre, L., R. Durazo, J. M. Hernandez-Ayon, F. Delgadillo-Hinojosa, G. Cervantes-Diaz, J. R. Lara-Lara, V. Camacho-Ibar, A. Siqueiros-Valencia, and C. Bazan-Guzman (2010), Temporal variability of the physical and chemical water characteristics at a coastal monitoring observatory: Station ENSENADA, *Cont. Shelf Res.*, *30*(16), 1730–1742, doi:10.1016/j.csr.2010.07.011.

Lynn, R. J., and J. J. Simpson (1987), The California Current System: The seasonal variability of its physical characteristics, *J. Geophys. Res.*, *92*(C12), 12,947–12,966.

McClatchie, S., R. Goericke, R. Cosgrove, G. Auad, and R. Vetter (2010), Oxygen in the Southern California Bight: Multidecadal trends and implications for demersal fisheries, *Geophys. Res. Lett.*, *37*, L19602, doi:10.1029/2010GL044497.

Min, D.-H., J. L. Bullister, and R. F. Weiss (2002), Anomalous chlorofluorocarbons in the Southern California Borderland Basins, *Geophys. Res. Lett.*, *29*(20), 1955, doi:10.1029/2002GL015408.

Nam, S., H.-J. Kim, and U. Send (2011), Amplification of hypoxic and acidic events by La Niña conditions on the continental shelf off California, *Geophys. Res. Lett.*, *38*, L22602, doi:10.1029/2011GL049549.

Ohman, M. D., B. E. Lavaniegos, and A. W. Townsend (2009), Multidecadal variations in calcareous holozooplankton in the California Current System: Thecosome pteropods, heteropods, and foraminifera, *Geophys. Res. Lett.*, *36*, L18608, doi:10.1029/2009GL039901.

Orr, J. C., et al. (2005), Anthropogenic ocean acidification over the twenty-first century and its impact on calcifying organisms, *Nature*, *437*(7059), 681–686, doi:10.1038/nature04095.

Peterson, B., et al. (2006), The state of the California current, 2005–2006: Warm in the north, cool in the south, *CCOFI Rep.*, *47*, 30–74.

Pierrot, D., E. Lewis, and D. W. R. Wallace (2006), MS Excel program developed for CO_2 system calculations, *Rep. ORNL/CDIAC-105a*, Carbon

Dioxide Inf. Anal. Cent., Oak Ridge Natl. Lab., U.S. Dep. of Energy, Oak Ridge, Tenn.

Raymond, P. A., J. E. Bauer, N. F. Caraco, J. J. Cole, B. Longworth, and S. T. Petsch (2004), Controls on the variability of organic matter and dissolved inorganic carbon ages in northeast US rivers, *Mar. Chem.*, *92*(1–4), 353–366, doi:10.1016/j.marchem.2004.06.036.

Rykaczewski, R. R., and J. P. Dunne (2010), Enhanced nutrient supply to the California Current Ecosystem with global warming and increased stratification in an earth system model, *Geophys. Res. Lett.*, *37*, L21606, doi:10.1029/2010GL045019.

Scripps Institution of Oceanography (2007), A compilation of the physical, chemical, and biological data for the winter 2005 CalCOFI Cruise, *Data Rep. CalCOFI Cruise 0501*, La Jolla, Calif.

Thomson, R. E., and M. V. Krassovski (2010), Poleward reach of the California Undercurrent extension, *J. Geophys. Res.*, *115*, C09027, doi:10.1029/2010JC006280.

Todd, R. E., D. L. Rudnick, R. E. Davis, and M. D. Ohman (2011), Underwater gliders reveal rapid arrival of El Nino effects off California's coast, *Geophys. Res. Lett.*, *38*, L03609, doi:10.1029/2010GL046376.

Wootton, J. T., C. A. Pfister, and J. D. Forester (2008), Dynamic patterns and ecological impacts of declining ocean pH in a high-resolution multi-year dataset, *Proc. Natl. Acad. Sci. U. S. A.*, *105*(48), 18,848–18,853, doi:10.1073/pnas.0810079105.